Understanding the Channel Busy Ratio Metrics for Decentralized Congestion Control in VANETs

Alessia Autolitano†, Massimo Reineri†, Riccardo M. Scopigno†, Claudia Campolo*, Antonella Molinaro*
†Istituto Superiore Mario Boella, Turin, Italy – E-mail: surname@ismb.it
*Università Mediterranea di Reggio Calabria, Italy – E-mail: name.surname@unirc.it

***Abstract*—Most of the emerging applications for road safety and traffic management rely on the frequent exchange of awareness messages among vehicles. Unfortunately, the 802.11 protocol poorly behaves under congested scenarios and cannot guarantee the reliability and timeliness demands of massively transmitted broadcast messages, leading to the severe degradation of safety.**

Recently, there has been a consensus from academia, automotive industries and standardization bodies in adapting transmission parameters (e.g., rate, transmission power) according to the channel load status. Although the objective of controlling channel load can be met with *local load measurements only*, the participation and fairness principles require the dissemination and sharing of load information among vehicles.

In this paper, we aim to shed light on the dynamics of the *channel busy ratio* (CBR) metrics (locally measured and shared over one/two hops), commonly used in the literature and at the basis of the Decentralized Congestion Control (DCC) standard, under different density and mobility settings.

***Index Terms*—CAM, congestion control, DCC, ETSI, channel busy ratio, VANET**

I. Introduction

Vehicular ad hoc networks (VANETs) are expected to play a crucial role in future Intelligent Transportation Systems (ITS). A wide set of applications aimed to prevent collisions and improve transportation efficiency can be supported by enabling communication between vehicles.

Cooperative Awareness Messages (CAMs), aka Basic Safety Messages (BSM) in US, have been introduced in Europe [1] to this purpose. They are regularly transmitted in broadcast (with a frequency ranging from 1 to 10 Hz) on the safety channel (Channel 172 in US, the Common Control Channel in Europe) [2] to provide real-time information of a vehicle presence, position and basic status to one-hop neighbors. By receiving CAMs, a vehicle can promptly recognize an abnormal maneuvering of the surrounding vehicles such as a hard brake situation and notify the driver to react accordingly.

It is well known that the performance of the standard IEEE 802.11 protocol [3] for inter-vehicular communication heavily degrades as the network load increases. Congestion on the safety channel has the dramatic effect of increasing the CAM loss probability and makes it more difficult for a vehicle to recognize potentially dangerous situations in its neighborhood.

Several works have addressed congestion mitigation techniques in VANETs [4]-[5]. In 2011 ETSI (European Telecommunications Standard Institute) has specified a set of Decentralized Congestion Control (DCC) mechanisms [6] that adapt transmission parameters to keep the channel load below predefined thresholds. The works in [7]-[8] have investigated the performance of DCC, by asserting that it poorly behaves with its initially conceived settings and fails to effectively meet latency and delivery requirements of CAMs.

A new standardization phase has been started and is still underway [9], expected to publish a new draft by the end of 2014. The ongoing DCC design lays its foundations into the works in [10] and [11]. It proposes a message rate control algorithm as LIMERIC in [10] to allow the total channel load to remain below a specific threshold. It inherits from the PULSAR mechanism in [11] the concept of sharing channel load information to avoid unstable system behavior. The nodes piggyback into transmitted safety messages the channel busy ratio *(CBR) information over two hops*, so that they can converge to the same message rate of the most congested node.

Nonetheless the preliminary evaluation studies showing the stability and fairness properties of the integrated solution [12], a comprehensive and detailed analysis of the CBR metrics at different hops, used as inputs to the DCC rate adaptation mechanism, is still missing. In order to fill this gap, this paper aims to provide the following contributions:

- to investigate the relationships between the CBR *locally perceived by vehicles*, the *one-hop CBR*, representing the locally perceived value reported by one-hop neighbors and *the two-hops CBR*, representing the one-hop CBR as reported by one-hop neighbors, under different settings;
- to assert the correlation of the *local CBR*, the *one-hop CBR* and *the two-hops CBR* with the one-hop and two-hops neighborhood of vehicles;
- to shed light on the impact that vehicles' position and mobility in a urban grid with intersections and obstructions may have on the computation of the CBR metrics.

Such contributions would be particularly relevant at this stage of DCC deployment: since the overall DCC is being re-discussed, a deeper insight into the CBR metrics is critical to provide guidelines for the ongoing standardization efforts. The remainder of the paper is organized as follows. Solutions relying on the CBR metrics to mitigate congestion are scanned in Section II, while Section III shortly describes the newly conceived DCC mechanism. Motivations and objectives of the work are provided in Section IV. Section V presents the performance evaluation criteria, simulation settings and metrics; results are analyzed in Section VI, while the conclusive remarks are wrapped up in Section VII.

978-1-4799-6729-2/14/$31.00 ©2014 IEEE

DOI 10.1109/ICCVE.2014.126

II. The channel load metrics in vehicular congestion control algorithms

Techniques proposed in the literature to mitigate congestion in VANETs adapt the transmission power, the packet transmission interval, the carrier sense threshold, or jointly some of (all) these parameters. This is typically done according to the channel load conditions. The majority of work estimates the load on the channel through the CBR metric that returns the ratio when the channel was reported busy from the access layer in a given time interval. CBR proved to be a suitable metric to increase packet delivery performance [5]. Some works rely on local CBR measurements only, while others let vehicles share channel state information to accurately capture the overall environment conditions. In [4] a distributed algorithm is proposed that adjusts the transmission power of nodes so that the local channel load goes below a pre-defined threshold. The same objective is targeted by reducing the transmission rate for a vehicle and adapting jointly transmission power and packet interval, in [10] and [13], respectively.

Channel load measurements are also driving the DCC standard. The first release by ETSI in July 2011 [6] includes mechanisms that, based on the CBR, adapt the transmission power, the packet interval, the data rate, and the sensing threshold of *Clear Channel Assessment* (CCA). Such mechanisms rely on a state machine that evolves, based on the channel load status, from *relaxed*, to *active*, and to *restrictive*, in increasing order of congestion. State transitions are triggered when the CBR *as locally perceived by each vehicle* exceeds/goes below given thresholds for a period of time.

Authors in [14] recognize local and global oscillation of the state machine, hindering vehicles to access the channel in some cases and leading to increased latency. Results in [8] confirm that DCC has poor performance and show that controlling message rate and transmission power has a major effect on the DCC behavior.

The identified weaknesses of the initially conceived DCC mechanisms, along with the recent works arguing the need for channel load information sharing, motivated the stakeholders involved in the standardization process to investigate a different solution. Work is underway for the definition of a new DCC mechanism, v1.1.2, [9], that lays its foundations into the solutions proposed in [10] and [11].

In [11] the packet transmission rate is adapted based on a comparison between the measured channel load and a pre-defined threshold. The authors propose an information dissemination technique to let neighboring vehicles share their CBR measurements. Because of fading, neighbors can come to different assessments of the channel state, then exchanging channel state information ensures participation and fairness principles. They even propose to piggyback the CBR information *over two hops*, because, under uniform transmission range hypothesis, it is not possible to notify all nodes within the physical carrier sense range (approximately twice the theoretical transmission range) by using one-hop piggybacking only.

III. DCC v1.1.2 in a nutshell

The newly conceived DCC at the *Access* layer adapts the message rate as in [10], according to CBR measurements. The CBR is measured through a service primitive, called *PHY_CCA.indication*, available at the PHY layer of IEEE 802.11 [3] for CCA to convey the channel status (busy or not) to the MAC layer.

The DCC algorithm is triggered every T_{CBR} interval, when a new value of the *local CBR*, CBR_0[1], is delivered from the chipset. The local CBR is computed as $T_{CCA-BUSY}/T_{CBR}$, where $T_{CCA-BUSY}$ is the time the channel was busy according to the *PHY_CCA.indication* during the T_{CBR}.

The task of CBR information sharing is demanded to the *GeoNetworking* protocol [15] at the network & transport layer. Each node sends to its neighbors: *(i)* its view of congestion based on the last local CBR measurement (CBR_0) and *(ii)* the maximum CBR value it has received from the one-hop neighbors (CBR_1). The resulting CBR_{DCC} parameter, used in the Access Layer, considers measurements taken locally and in the neighborhood and it is computed as follows:

$$\text{CBR}_{DCC} = max(\text{CBR}_0, \text{CBR}_1, \text{CBR}_2) \tag{1}$$

with CBR_1 and CBR_2 being, respectively, the *maximum* CBR_0 (i.e., the *one-hop CBR*) and CBR_1 (i.e., the *two-hops CBR*) values received from neighboring nodes in a given T_{CBR} interval.

The DCC algorithm is executed and computes the minimum time between successive packets generation, *T_GenPacket_DCC*, that is equal to $1/$*ego_target_rate*. The *ego_target_rate* r [2] for a vehicle j is computed as follows:

$$\begin{aligned} r_j(t) &= (1-\alpha) r_j(t-1) + \\ &+ sign(r_g - r_c(t-1)) \cdot min\left[X, \beta \cdot |r_g - r_c(t-1)|\right] \end{aligned} \tag{2}$$

where r_g is the *target_rate* (i.e., the aggregated rate), r_c is the total perceived rate by the local ITS station, X is set to 1, α to 0.1, and β to 1/150.

IV. Motivations and Objectives

The main objective of this study is to achieve a deeper understanding of the behavior of the channel busy ratio measurements. Given the crucial role of CBR metrics, locally computed and shared at one/two-hops, to provide feedback to control network congestion, it is mandatory to accurately capture their dynamics. The study aims to assess differences between the mentioned CBR metrics and to identify their possible dependencies on topology parameters, such the vehicle position and the number of one and two-hops neighbors. The analysis will be conducted in urban obstructed scenario, to better figure out the variations of the CBR metrics as a vehicle moves close to intersections.

Since any CBR value is only meaningful considering the underlying CCA threshold [11], the effect of its setting is also evaluated.

In addition to mutual relationships that can be somehow intuitively inferred and also observed through graphical inspection, the work harnesses a consolidated mathematical tool

[1]Notations have been simplified and shortened w.r.t the ones in [9].

[2]The DCC algorithm converts the CBR to messages/second by considering an average message size of 400 bytes transmitted at the default 6 Mbps rate. Then a 100% CBR corresponds to 2000 messages/second [10]. So, in eq. (2) $r_c = \text{CBR}_{DCC} \cdot 2000$, $r_g = \text{CBR}_{maximum} \cdot 2000$.

TABLE I: SIMULATION PARAMETERS

CATEGORY	PARAMETER	VALUE
PHY	Frequency/Channel bandwidth	5.9 GHz / 10 MHz
	Propagation	Nakagami (m=3)
	Power monitor threshold	-102 dBm
	Noise floor	-99 dBm
	CCA Threshold	(-65, -75, -85, -95) dBm
	Transmitted Power	20 dBm
MAC	Slot time/SIFS/Header length	13 μs / 32 μs / 40 μs
	Data rate/Contention window	6 Mbps / 15
DCC	T_{CBR}	100 ms
APP	Message interval/Payload size	100 ms / 400 Bytes

to quantitatively carry out this analysis, which is correlation. For the sake of precision, several correlation indexes have been defined in literature; the most common among them is the Pearson's one, and will be used also here.

V. EVALUATION CRITERIA AND METHODOLOGIES

Performance has been evaluated through *ns*-2 simulations with the overhauled PHY and MAC layers in [16].

The simulated topology includes a set of vehicles uniformly placed in a 750-m wide grid of 6x6 double lane roads, spaced 150 m apart, with buildings that prevent Line-of-Sight (LoS) propagation except along the straight roads. The RUG propagation model [17] is applied to consider the effect of obstructions on the received signal power.

Both static and dynamic scenarios, with fixed and mobile nodes respectively, are analyzed. In the static scenario, the CBR measurements are performed with an increasing number of fixed nodes (150, 300, 600, 900, 1200, 1800, 2400) in order to assess the behavior at different node densities. The mobility trace, generated by SUMO [18], includes 451 nodes, moving at a mean speed of 60 Km/h during a time interval of 40 s. The main simulation parameters, set according to standard specifications [3], [9], are summarized in Table I.

A. Premises about performance metrics based on correlation

Given a set of cardinality n, whose elements i are characterized by two variables x_i, y_i, the Pearson's correlation index, p, is defined as follows:

$$p = \frac{\sum_{i=1}^{n}(x_i - \bar{x})(y_i - \bar{y})}{\sqrt{\sum_{i=1}^{n}(x_i - \bar{x})^2 \sum_{i=1}^{n}(y_i - \bar{y})^2}}, \qquad (3)$$

where $\bar{x}$ and $\bar{y}$ are respectively the first momenta of the two variables. Typically a strong correlation is recognized when $|p| > 0.7$ and a weak correlation when $0 < |p| < 0.3$.

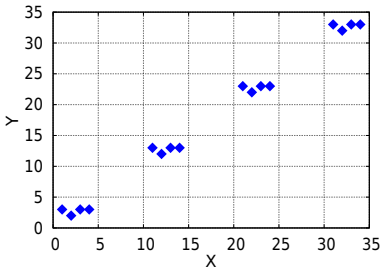

Fig. 1: Impact of the correlation domain on the results (an example).

In order to correctly compute correlation, a brief discussion will shortly introduce some intuitive properties of Pearson's correlation with a pragmatic approach, just to prevent that results may get distorted, especially when some statistical misbehavior becomes predominant.

Proposition 1: Correlation domain **- The domain of correlation may strongly influence the correlation result**. Dependencies tend to be stronger if viewed over a wider range of values. Take the example of Fig. 1 and its variables X and Y: when considering the only range $[1-4]$ of X the correlation is 0.25 (very weak) while, considering the full domain, it grows as high as 0.999. For this same reason, several techniques that attempt to correct for range restriction in one or both variables have been developed, especially for meta-analysis; the most known are Thorndike's case II and case III equations [19].

Proposition 2: Linearity **- Pearson's correlation is a metrics of how much strong is the direct (increasing) *linear* relationship between two variables**. This means that, if correlation is ± 1, there is a perfect linear relationship between two (samples are on a line with a positive slope if $p = +1$, with negative slope if $p = -1$). But this also means that $p = 0$ when all the samples are on a horizontal or vertical line and, also, p will get close to 0 when the samples tend to reach an asymptotic value. Additionally, even if a dependence is perfect but non-linear, the correlation may drop to zero, as in the case of samples uniformly spaced and perfectly matching a symmetric arc of a parable. In case of non-linear behaviors, some adjustments to the correlation may be needed.

Proposition 3: Distribution of Samples **- In case of non-perfect correlation between two variables, samples need to be uniformly spread over the correlation domains**. To explain this statement, consider again the example of Fig. 1. Here there is a strong correlation but it is not perfect, while the samples are evenly distributed over decades: the correlation is almost perfect (0.999). But, considering as many as 3 times the samples in the range $[11-14]$ (counting them 3 times, for instance), the correlation drops to 0.7.

B. Correlation computation in the simulated scenarios

All the analyses carried out in this paper address, in particular, the relationships between the different flavors of CBR (CBR_0, CBR_1, CBR_2) and the number of neighbors, considering two possible cases: neighbors at 1-hop distance (NH_1) and at two hops (NH_2). Hence, all the results will study CBR_0, CBR_1, CBR_2, NH_1 and NH_2: these are the *variables*. The set of 1 hop neighbors of a given node contains all the nodes that could potentially receive a packet from it. Indeed, knowing the transmission power and the position of the nodes, it is possible to compute the power attenuation, due to the fading and the presence of the obstructions (described through Nakagami and RUG propagation models, respectively). Consequently, for each vehicle, NH_1 is the number of the nodes that could receive the packets with a *Signal to Interference plus Noise Ratio* (SINR) higher than a threshold, depending on the modulation scheme; NH_2 is obtained from the 1 hop neighbors sets of all the direct neighbors.

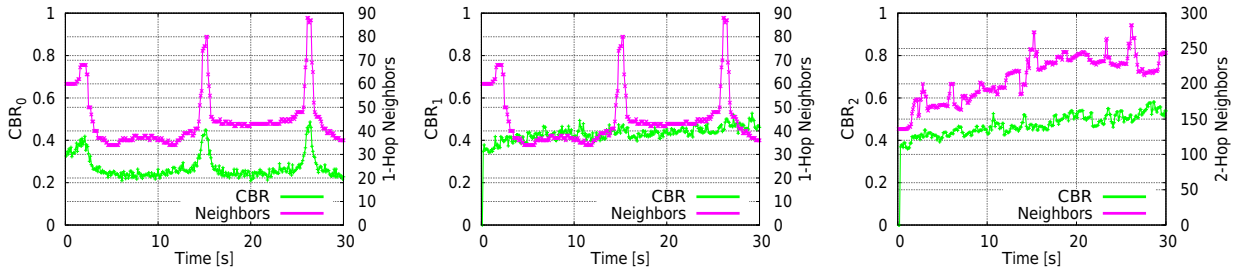

(a) CBR_0 and NH_1 (b) CBR_1 and NH_1 (c) CBR_2 and NH_2

Fig. 2: Details for Node 188. (a), (b), (c): Dependency on time of CBR and NH

The correlation in the mobility scenario is computed node by node, over time, while moving in the urban grid - so to point out the possible role of position; in the stationary scenarios, involving different densities of nodes, the correlation is computed independently of time (that is, at a given time for a certain number of nodes). In both cases, results are described *both* through the scattering graphs *and* (not only by) the correlation index, so to highlight possible violations to the previous propositions.

In the case of static nodes, the multiple densities (nodes are from 150 to 2400) adhere the indication of Proposition 1: a significant domain of next-hop nodes is covered, sufficient to underline dependencies (the interpolation will be in fact quite intuitive), while the overlapping between subsets of samples will be almost negligible (especially when far from the saturation). In order to cope with Proposition 3, in all the scenarios, independently of the respective number of simulated nodes, only 100 of them (the ones closest to the center, so to limit border effects) will be considered. Finally, as far as Proposition 2 is concerned, attention will be paid to the possible influence of a non-linear distribution of samples on the computation of correlation, so to distinguish - if needed - between *Pearson's correlation* and *dependency*.

VI. Simulation Results

As anticipated, the first set of results concerns the analysis of how the CBR variables are influenced by the node mobility and position in the Manhattan grid.

This study focuses on the nodes that are in motion for the most of the simulation time, remaining stationary for a consecutive period no longer than 10 seconds. This is because, otherwise, their scarce mobility would have a non negligible impact on the channel load evaluation. Several nodes that verify this property have been identified. In Fig. 2 and Fig. 3, one of them, the node 188, is tracked over a period of 30 seconds. In Fig. 2(a)-(c) the CBR_0, CBR_1 and CBR_2 are compared to the number of one-hop and two-hops neighbors; in Fig. 3(b) the trajectory for node 188 in the grid can be seen (it is a straight path covering 3 crossroads); in Fig. 3(a) the variation in the node speed is plotted. The peaks in the number of neighbors (Fig. 2(a)-(b)) correspond to the time when a crossroad is met; while they are well reflected by the CBR_0 - as expected - they do not leave traces either on CBR_1 or CBR_2. Indeed, the attenuation of the wireless signal changes when passing from Non-LoS to LoS conditions as approaching the center of the crossroad, with consequent effect on the locally measured CBR. Additionally, CBR_1 is *almost the same* and CBR_2 is *the same* for all the nodes: it means that the whole map is covered with two hops; additionally, given the $\max()$ operator in the CBR_1 definition, all the nodes perceive the same channel busy ratio. On the other hand, if the CBR_2, in particular, is the same for all the nodes, one would expect a steady line, while in Fig. 2(c) a smooth speed increase is visible (from less than 0.4 to about 0.5). A careful analysis revealed that SUMO trace tends to have less nodes in the borders of the map: in fact the mean distance from the center decreases from 320 m down to 280 m; this is sufficient to justify a slightly higher and growing density, hence a little bit higher CBR_2 over time.

This first scenario, altogether, shows that only CBR_0 is significantly dependent on the node position in the reference grid and that this measurement is strongly related to the number of neighbors.

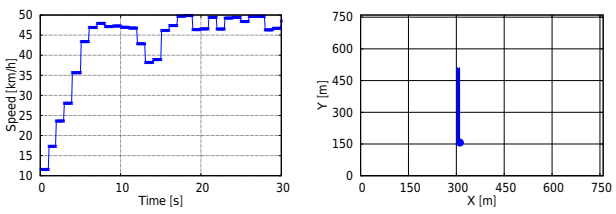

(a) Speed (b) Trajectory

Fig. 3: Kinematics details for Node 188.

TABLE II: Correlation indexes for Node 188:

CBR_i	NH_j	p	CBR_i	NH_j	p
0	1	0.923	0	2	-0.298
1	1	0.292	1	2	-0.176
2	1	0.181	2	2	-0.129

The correlation indexes are computed node by node and on the average of nodes for any couple of variables (CBR_i, NH_j). The results, summarized in Table II for the node under analysis, show that the only relevant (and high) correlation found is the one between CBR_0 and NH_1. Even more, this correlation varies significantly node by node (between 0.8 and 0.9) and it seems strange that no correlation ($|p| < 0.3$) may be identified for the other variables. Here, the Propositions 1 and 3 provide the correct interpretation. When correlating samples over time as in the two plots in Fig. 2(b), a too narrow domain in the CBR_1 is considered, around 0.4 (Proposition 1) and, additionally, the intervals are over-sampled (Proposition

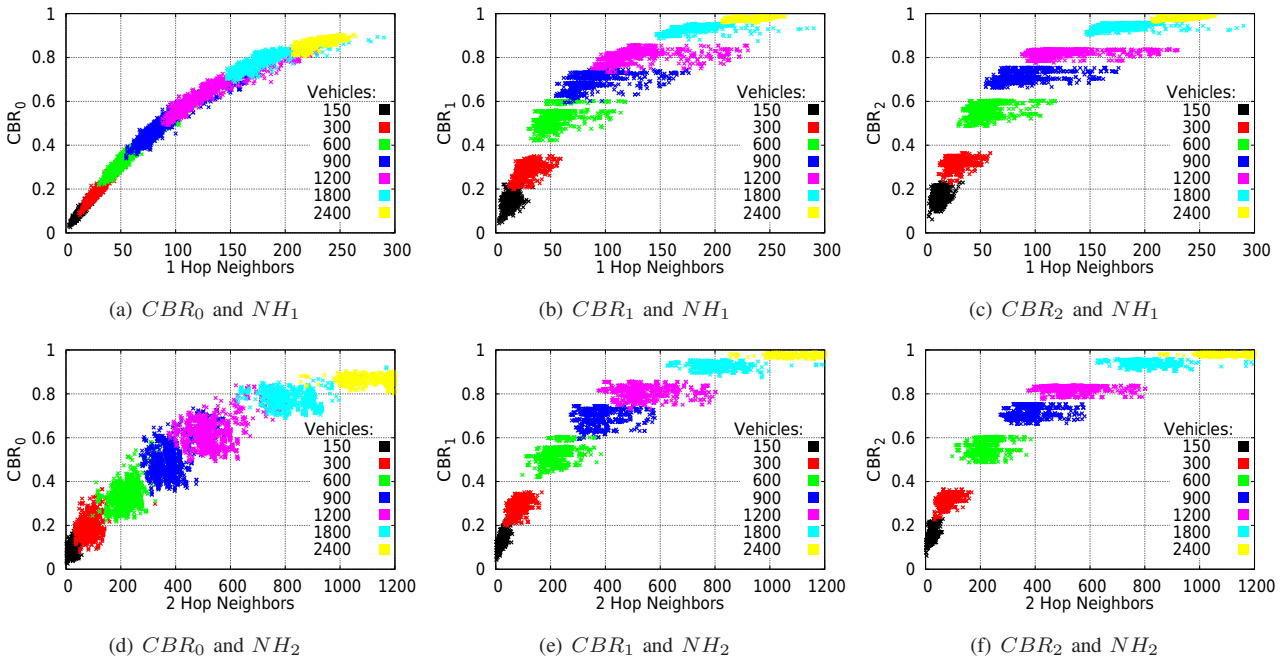

(a) CBR_0 and NH_1 (b) CBR_1 and NH_1 (c) CBR_2 and NH_1

(d) CBR_0 and NH_2 (e) CBR_1 and NH_2 (f) CBR_2 and NH_2

Fig. 4: Scattering plots for the analysis of the CBR and NH variables and their correlations (CCA threshold is equal to -85 dBm)

3) when the number of neighbors is lower (one spends less time in the centers of the crossroads). The latter holds also for the correlation between CBR_0 and NH_1, which might grow even more. Summing up, it is needed a more extensive and different approach to analyze such open issues.

For this purpose, a rich set of simulations, under very different load conditions, has been run. In this case, the focus is on the same variables but independently of time and position, with the purpose of covering the correlation domain as extensively as possible. For the reasons explained in subsection V-A, the simulations include several static scenarios with an increasing number of nodes, each repeated 10 times using different seeds. At a predefined time (30s) the most central 100 nodes are considered for each simulation and their variables respectively averaged across 10 runs.

All the plots in Fig. 4 are meant as correlation graphs, so to let identify the existing relationships between one among CBR_0, CBR_1 and CBR_2 and one between NH_1 and NH_2. In each graph, the scattered points highlight, color by color, the results coming from a scenario with a different number of nodes. When using the same X domain (e.g., number of neighbors at 1 hop), the same x coordinate will represent the same node in all the graphs (respectively CBR_0, CBR_1 and CBR_2).

All the graphs, whose y-axis is some kind of CBR, show an obvious saturation to one, which is intrinsic in the CBR metrics (it cannot exceed 1, by definition). Additionally, there is a clear non-decreasing trend in all the scatterings and a function like a $\tanh(Ax)$ is intuitively a good curve for the regression of each graph. The slope is higher as the order of CBR (CBR_0, CBR_1, CBR_2) increases and this is quite intuitive: in fact CBR_1 is the maximum value of CBR by all the neighbors; in other words: as soon as a node i perceives a higher CBR_0 (say CBR_0^i), all its neighbors k_i will have a $\text{CBR}_1^{k_i} \geq \text{CBR}_0^i$).

Specifically for the plots concerning 1-hop neighbors (Fig. 4.(a)-(c)), the previous effect also implies that the higher the CBR order the more the curves get squeezed in their co-domain: more and more nodes will measure the same CBR, independently of the number of nodes at 1-hop distance, intrinsically due to the way the CBR is computed (it is related to a maximum). This also lowers the degree of correlation and makes the scatter graphs less continuous (the scattered points highlight some gaps).

When considering the number of neighbors at two hops, more or less, the same effects hold.

TABLE III: CORRELATION INDEXES: p AND p^*

CBR_i	NH_j	p	$p*$	CBR_i	NH_j	p	$p*$
0	1	0.975	0.985	0	2	0.948	0.966
1	1	0.921	0.948	1	2	0.910	0.941
2	1	0.913	0.942	2	2	0.904	0.937

Once achieved this understanding, the correlation can be computed for all the six scattering plots and the results are shown in Table III. In order to evaluate the impact of non-linear behaviors due to the CBR saturation (Proposition 2), two versions of p have been computed: the one using all the samples (p) and one (p^*) obtained considering only the less populated scenarios (up to 900 nodes, no more) - so to neglect the impact of non linear regression of the samples.

Results are all greater than 0.9, meaning that the correlation for any couple $(\text{CBR}_i, \text{NH}_j)$ is strong. As expected, the highest value is obtained with $(\text{CBR}_0, \text{NH}_1)$, reflecting the appearance of the scattering plot. Additionally, passing to the version p^*, no dramatic improvement is met: this is ascribed to two reasons. First of all, the samples coming from the scenario with 2400 nodes do not displace too much the overall set of samples in the area characterized by CBR; secondly, for the sake of precision, the more p approaches 1, the more it is difficult to improve it: so, at over 0.9 significant improvements

in the graphs (with a lower scattering and a more linear trend) only lead to small increase of the index p.

Observing the two sets of results obtained under mobility and with a fixed topology, it is possible to detect correlation between all the curves, but usually it is perceivable on a larger scale than in a single scenario. However, the correlation between the variables $(\mathrm{CBR}_0, \mathrm{NH}_1)$ is so strong that can be revealed just by a single simulation: due to the obstructions and to the lack of multi-hop phenomena (both in CBR_0 and in NH_1), a single simulation covers sufficiently wide domain and co-domain. Besides, their evolution over time (Fig. 2(a)) shows the strongest dependency, highlighting also local effects due to the shadowing by the buildings.

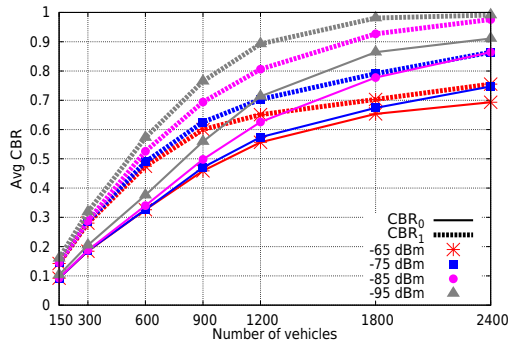

Fig. 5: A final comparison between CBR_0 and CBR_1, also considering different possible CCA threshold values

Eventually the comparison between CBR_0 and CBR_1 at different traffic loads has been studied (Fig. 5), also considering different possible CCA levels. In all the cases, since CBR_1 and CBR_2 are quite close, CBR_2 measures are not depicted to make the graph clearer. Obviously, the lower the CCA threshold and/or the higher the CBR order, the higher the perceived CBR will be. And, unless the density becomes very high (1200 vehicles or more), the step from CBR_0 to CBR_1 leads to more dramatic effects than lowering the sensitivity from -65 dBm to -95 dBm.

Summing up, the main difference occurs between CBR_0 and CBR_1, with the former able to show (or affected by) local effects due to a very strong correlation to the number of nodes in the same radio range; the latter inherits a more global meaning and lets all the nodes be aware of the maximum CBR in the radio range. CBR_1 is potentially useful to upper-bound the effects of hidden terminals, since all the nodes would know what CBR is perceived by the vehicles in the centers – the one more exposed to collisions under heavy load [17].

On the other hand, it also seems to grow to saturation in a very rapid way, potentially affecting the overall stability of DCC. This aspect deserves additional investigation, first of all by closed-loop simulations, involving the mutual influence by CBR computation on DCC mechanisms and *vice-versa*.

VII. Conclusion

CBR is the one of the cornerstones of the new DCC. It has been here analyzed considering, in particular, obstructed scenarios with different settings: this has permitted to achieve a significant awareness on its characteristics through a rich set of simulations, addressing the analysis of correlation between the channel busy ratio and the number of neighbors.

Some open points have been already identified and deserve additional investigations: the main two concern (*i*) the assessment of CBR metrics in closed-loop scenarios involving also DCC and (*ii*) the impact of other types of obstructions, that is obstructions by vehicles (which may significantly affect the differences among CBR_i criteria) and by non regular urban topologies. They will be both addressed by our future studies.

Acknowledgements

The FP7 project GLOVE (joint GaliLeo Optimization and VANET Enhancement G.A.287175) has supported this study. GLOVE aims at identifying VANETs weaknesses and at mitigating them by leveraging the time-space information provided by Galileo (WP1, WP2).

References

[1] ETSI EN 102 637-2, "ITS; Vehicular Communications; Basic Set of Applications; Part 2: Specification of Cooperative Awareness Basic Service," June 2012.
[2] C. Campolo, A. Molinaro, "Multichannel Communications in Vehicular Ad Hoc Networks: A Survey," *IEEE Comm. Magazine*, vol. 51, no. 5, pp. 158-169, 2013.
[3] IEEE Std. 802.11-2012: "IIEEE Standard for Information technology - Telecommunications and information exchange between systems - Local and metropolitan area networks-Specific requirements - Part 11: Wireless LAN Medium Access Control (MAC) and Physical Layer (PHY) Specifications"
[4] M. Torrent-Moreno, et. al., "Vehicle-to-vehicle communication: fair transmit power control for safety-critical information," *IEEE Trans. on Vehi. Tech.*, vol. 58, no. 7, pp. 3684-3703, 2009.
[5] Y. P. Fallah, C. Huang, R. Sengupta, and H. Krishnan, "Analysis of Information Dissemination in Vehicular Ad-Hoc Networks With Application to Cooperative Vehicle Safety Systems," *IEEE Trans. on Vehicular Technology*, vol. 60, no. 1, pp. 233247, Jan. 2011.
[6] ETSI TS 102 687 V1.1.1, "Intelligent Transport Systems (ITS); Decentralized Congestion Control Mechanisms for Intelligent Transport Systems operating in the 5 GHz range; Access layer part," July 2011.
[7] S. Subramanian, et. al., "Congestion Control for Vehicular Safety: Synchronous and Asynchronous MAC Algorithms," *ACM VANET* 2012.
[8] A. Autolitano, C. Campolo, A. Molinaro, R.M. Scopigno, A. Vesco, "An insight into Decentralized Congestion Control techniques for VANETs from ETSI TS 102 687 V1. 1.1," *IEEE/IFIP Wireless Days (WD)* 2013.
[9] Draft TS 102 687 V1.1.2, "Intelligent Transport Systems (ITS); Decentralized Congestion Control Mechanisms for Intelligent Transport Systems operating in the 5 GHz range; Access layer part," January 2014.
[10] J. Kenney, et. al., "LIMERIC: A Linear Message Rate Control Algorithm for Vehicular DSRC Systems," *IEEE VNC*, 2011.
[11] T. Tielert, et. al., "Design Methodology and Evaluation of Rate Adaptation Based Congestion Control for Vehicle Safety Communications," *IEEE VNC*, 2011.
[12] G. Bansal, et al. "EMBARC: error model based adaptive rate control for vehicle-to-vehicle communications," *ACM VANET* 2013.
[13] L. Le, et. al., "Performance Evaluation of Beacon Congestion Control Algorithms for VANETs," *IEEE GLOBECOM*, 2011.
[14] D. Eckhoff, N. Sofra, R. German, "A Performance Study of Cooperative Awareness in ETSI ITS G5 and IEEE WAVE," In *IEEE WONS 2013*.
[15] ETSI TS 102 636-4-2 V1.1.1, "Intelligent Transport Systems (ITS); Vehicular Communications; GeoNetworking; Part 4: Geographical addressing and forwarding for point-to-point and point-to-multipoint communications; Sub-part 2: Media-dependent functionalities for ITS-G5," October 2013.
[16] Qi. Chen, et al. "Overhaul of IEEE 802.11 Modeling and Simulation in NS-2," *ACM MSWiM* 2007.
[17] H.A. Cozzetti, C. Campolo, R.M. Scopigno, A. Molinaro, "Urban vanets and hidden terminals: Evaluation through a realistic urban grid propagation model," *IEEE International Conference on Vehicular Electronics and Safety (ICVES)*, 2012.
[18] "Simulation of Urban MObility (SUMO), http://sumo-sim.org,"
[19] Robert Ladd Thorndike, "Research problems and techniques (Report No. 3).," *US Govt. print. off.* 1947.